

## X-ray emission caused by Raman scattering in long-scale-length plasmas

R. P. Drake, R. E. Turner, B. F. Lasinski, E. A. Williams, Kent Estabrook, W. L. Kruer, and E. M. Campbell

*Lawrence Livermore National Laboratory, Livermore, California 94550*

T. W. Johnston

*Institut National de la Recherche Scientifique-Energie, Montreal, Quebec, Canada JOL 2PO*

(Received 8 September 1988)

By analysis of data from a specific set of laser-plasma interaction experiments, it is argued that stimulated Raman scattering (SRS) is responsible for the hard ( $> 30$ -keV) x rays emitted from the targets. The Novette laser [K. R. Manes *et al.*, *Laser Part. Beams* **3**, 173 (1985)] was used to irradiate thick, gold targets with up to 4 kJ of 0.53- $\mu\text{m}$  light in 1-ns, Gaussian pulses at average intensities of  $(1-200) \times 10^{14}$  W/cm<sup>2</sup>, producing approximately planar plasmas with temperatures of order 3 keV and density-gradient scale lengths of order 250  $\mu\text{m}$ . The spectrum, amplitude, and timing of the hard x rays emitted by the plasma were measured along with various properties of the scattered light. All the data are consistent with the hypothesis that SRS is the source of the hot electrons that emit the x rays, and some data conflict with any other plausible hypothesis.

### I. INTRODUCTION

In this paper we report a study of the hard ( $> 30$ -keV) x rays emitted from targets irradiated with up to 4 kJ of 0.53- $\mu\text{m}$  light in 1-ns pulses. The plasma produced by these irradiations, at intensities of order  $10^{15}$  W/cm<sup>2</sup>, was inferred to have a background electron temperature of about 3 keV and a density-gradient scalelength [ $L \equiv n(dn/dx)^{-1}$ ] of about 500 laser wavelengths at  $0.1n_c$ , where  $n_c$  is the critical density of the laser light.<sup>1</sup> The x rays were produced by bremsstrahlung emission in the dense matter behind the plasma. In the present work we report measurements of the x-ray spectrum, spectral intensity, and timing, as well as inferences of the temperature and energy content of the hot electrons that produced these x rays. We compare this evidence to measurements of the light scattered from the target, and conclude that stimulated Raman scattering (SRS) was responsible for most of the hot electrons that produced the x rays.

This research is of interest to plasma physics because hot electrons can be produced as a result of several interaction processes when a laser irradiates a plasma, leading to the question of which process dominates under what conditions. Any process that can produce or trap electron-plasma waves is a potential source of hot electrons. Such processes include resonance absorption,<sup>2,3</sup> the decay instability,<sup>4</sup> two-plasma decay,<sup>5,6</sup> caviton collapse,<sup>7</sup> and SRS.<sup>8</sup> In the present experiments, with relatively long scalelengths, planar plasmas, warm temperatures, and high laser intensities, SRS is shown to dominate.

In addition, this research is of interest to laser fusion, which hot-electron production can adversely affect. Hot electrons, with energies significantly above the thermal

electron temperature, could penetrate the laser-fusion capsule and preheat the fusion fuel. This would make the fuel more difficult to compress and would reduce the gain of a laser-fusion target.<sup>9</sup>

Hot electrons have been attributed to SRS in several previous papers. In large-scale-length, 1.06- $\mu\text{m}$  experiments with overdense targets,<sup>10</sup> the hot-electron fraction and temperature, inferred from the x-ray spectrum, was consistent with the production of the hot electrons by Raman scattering. Hot electrons have been attributed to Raman forward scatter by Joshi *et al.*,<sup>11</sup> and to Raman backscatter by Berger *et al.*<sup>12</sup> Both of these experiments used 10.6- $\mu\text{m}$  irradiation of underdense plasmas to produce the Raman scattering and the hot electrons. In addition, the present observation of efficient SRS and its correlation with hot electrons has been reported in Letter form.<sup>13</sup> The present paper presents more complete data and the results of several measurements that were not included in the Letter.

The experiments used the Novette laser<sup>14</sup> at the Lawrence Livermore National Laboratory to irradiate Au or Be targets with 0.53- $\mu\text{m}$  light in 1-ns, Gaussian pulses. The targets did not burn through during the laser pulse as was verified by measurements of the transmitted light and the scattered light in the forward hemisphere, and by images of the x-ray emission at  $\sim 2$  keV and at  $\sim 600$  eV. The energy on target was typically 3.5 kJ, and the average intensity,  $I_L$ , was decreased from  $2 \times 10^{16}$  to  $1.4 \times 10^{14}$  W/cm<sup>2</sup> by increasing the size of the laser spot from 150 to 1900  $\mu\text{m}$ . All but two of the experiments used intensities below  $4 \times 10^{15}$  W/cm<sup>2</sup>, with spot sizes above 380  $\mu\text{m}$ , producing plasmas that are inferred to remain approximately planar throughout the laser pulse. Further details of the experimental conditions are described in Ref. 1.

## II. THE X-RAY SPECTRUM

An absolutely-calibrated x-ray spectrometer measured the spectrum of the suprathreshold x rays. This spectrometer included several filter-fluorescer channels and several *K*-edge channels. The filter-fluorescer channels employ a prefilter, a fluorescer, and a post filter to obtain good energy resolution. The *K*-edge channels use *K*-edge filters along a line of sight to obtain more sensitivity but less resolution. Both types use scintillators and photomultiplier tubes as detectors.

The broad spectral response of these x-ray detectors implies that their sensitivity depends on the shape of the x-ray spectrum. As a result, the data do not uniquely determine the x-ray spectrum. However, one can find a physically plausible spectrum that is consistent with the data, in which case the signal amplitudes determine the spectral intensity of the x rays. We use an iterative computation to find a plausible spectrum. A computer program calculates the signal amplitudes that would result from a trial spectrum, compares these to the data, and iterates the shape and magnitude of the spectrum to make it more consistent with the data. Figure 1 shows the results for three of the gold-disk experiments. The data shown in Fig. 1(a) were from a low-intensity irradiation and produced few x rays. Only some of the *K*-edge channels obtained data. Figure 1(b) shows data from an irradiation producing more x rays, and Fig. 1(c) shows data from an irradiation that produced a comparatively large hard x-ray flux. For the data shown in Fig. 1(c), the x-ray spectrum below 20 keV is not meaningful because the diagnostic was behind the target and the spectrum of these low-energy x rays was significantly modified by passing through it. The data at energies above 20 keV do accurately represent the spectrum of harder x rays produced by bremsstrahlung of hot electrons in the 5- $\mu\text{m}$  thick, Au targets.

The simplicity of the observed spectra allowed us to simplify the routine analysis of the hard x-ray data. Note that in all the cases shown in Fig. 1, the spectrum above 40 keV is adequately represented by an exponential function with a single slope corresponding to an *e*-folding energy or "temperature" of order 20–35 keV. For spectra with this shape and temperatures in this range, the sensitivity of the channels does not vary significantly. As a result, we were able to use a trial spectrum with a temperature of 24 keV to reduce the data. The resulting spectral intensities were fit by eye with a single-slope x-ray spectrum of a similar temperature. The inferred temperatures, in 27 cases, ranged from 20 to 33 keV, with one experiment at 55 keV. We compared the results of this technique to those of the iterative procedure and evaluated the effects of uncertainties in the detector calibration to determine the uncertainty in the slope ( $\pm 20\%$ ) and the spectral intensity ( $\pm 50\%$ ) of the measured spectrum. (The temperature of 55 keV from one experiment is much more uncertain.)

The spectral intensity of the x rays increased strongly as the laser intensity increased. As Fig. 1 shows, a 40-fold increase of the laser intensity produced a 1000-fold increase of the spectral intensity of the x rays. Spectra from Be targets, irradiated at about  $10^{15} \text{ W/cm}^2$ , appear

similar to those shown, and have an intensity that is smaller by the ratio of the nuclear charge of Be to that of Au.

The inference of the spectral intensity into  $4\pi$  steradians from the measured intensity at one location introduces additional uncertainty when the properties of the hot electrons are evaluated. The spectral intensity shown as the ordinate in Fig. 1 is  $4\pi$  times the spectral intensity per steradian measured by the instrument. In order to minimize the error associated with this assumption, the instrument was placed  $60^\circ$  from the target normal. As a result, the total spectra intensity is correctly calculated if the x-ray emission is either isotropic or Lambertian. The error in the total spectral intensity, introduced by deviations of the angular distribution of the x rays from these limits, is probably smaller than either the errors in the

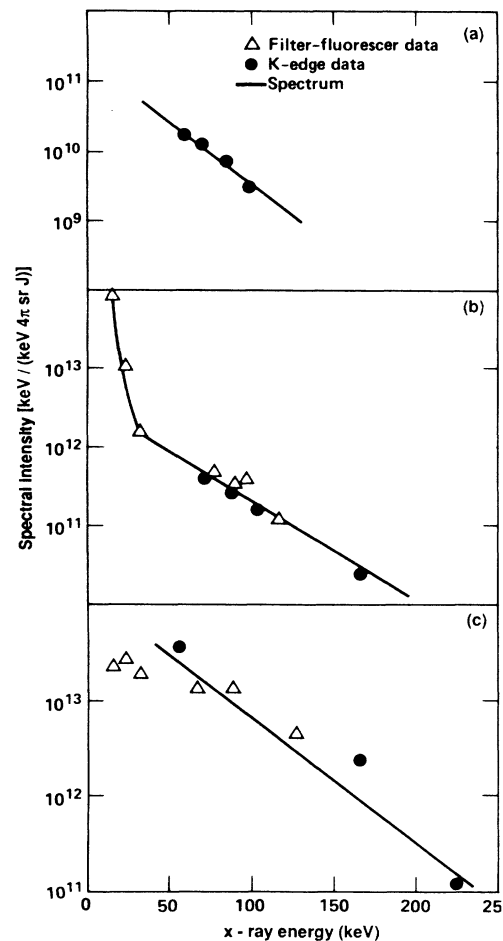


FIG. 1. The hard x-ray spectral intensity, in units of keV (keV  $4\pi$  Sr), is shown as a function of x-ray energy, for three experiments spanning a large variation in the fluence of the x rays. Each data shows the intensity inferred from a particular detector, assuming the shape of the spectrum corresponds to the solid line. The irradiating intensities and experiment numbers are (a)  $1.4 \times 10^{14} \text{ W/cm}^2$ , 93120212; (b)  $8.3 \times 10^{14} \text{ W/cm}^2$ , 93100603; (c)  $3.1 \times 10^{15} \text{ W/cm}^2$ , 94020303. The experiment numbers refer to the facility, year, month, day, and laser pulse number.

determination of the spectral intensity per steradian from the data (just discussed) or the errors in the inference of the energy content of the hot electrons from the x-ray spectrum.

The x-ray spectrum observed in the present experiments differs dramatically from that observed in a similar experiment using a smaller laser spot. Figure 2 compares the spectral intensity as a function of photon energy from one of the present experiments and from an experiment using the Argus laser. The Argus experiment used a 700-ps Gaussian pulse, a 70- $\mu\text{m}$ -diam laser spot, and about 30 J of laser energy (at 0.53  $\mu\text{m}$ ) to produce an intensity of about  $10^{15}$  W/cm<sup>2</sup>. The x-ray spectrum from Argus shows a slope of 11 keV. Its temperature and magnitude were easily explained<sup>15</sup> as the result of resonance absorption in this plasma with a small density-gradient scalelength ( $L/\lambda \sim 100$ ).

The spectrum from Novette was obtained with the same average laser intensity, beam quality, and target material, and almost the same pulse duration (1 ns versus 700 ps) as the spectrum from Argus, but with a laser spot that was ten times larger. The laser spot of the Novette irradiation was larger than  $c_s\tau$  (where  $c_s$  is the sound speed in the plasma and  $\tau$  is the duration of the laser pulse), while the laser spot of the Argus irradiation was smaller than  $c_s\tau$ . It is obvious from the figure that one or more interaction mechanisms causing hard x-ray emission were excited much more strongly in the longer scale length, more planar plasma produced by Novette.

Even without further analysis, Raman scattering is the most plausible source of the hot electrons that produced the x rays in the Novette experiment. Processes occurring near critical density, including resonance absorption, should be less effective in the longer-scale-length plasma produced by Novette. Two-plasmon decay is well above threshold in both cases, and the observed level of  $\frac{3}{2}\omega_0$  light did not change markedly. In contrast, the energy scattered by SRS, as a fraction of the incident laser energy, was 2 orders of magnitude larger in the Novette irradiation<sup>1</sup> than in that of Argus.<sup>16</sup>

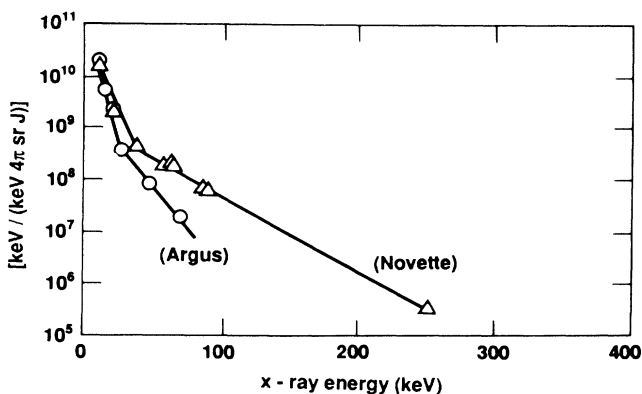


FIG. 2. The normalized x-ray spectral intensity, in units of  $\text{keV}/(\text{keV } 4\pi \text{ sr } J)$  incident on the target, is shown as a function of x-ray energy for two experiments, which differ principally in the size of the laser spot. The experiment with a larger laser spot produced more hard x rays.

### III. X-RAY TIMING

An optical streak camera with an S1 photocathode measured the relative timing of the optical and x-ray emissions. The photocathode was sensitive to x rays from 25 to 60 keV with a maximum sensitivity at 35 keV. The x-ray channel was protected from optical signals by a thin aluminum filter, and was sensitive enough to detect x rays when the fraction of the laser energy converted into hot electrons exceeded 1%. The optical channels were filtered using colored glass and interference filters. An optical fiducial allowed timing of the emissions, relative to the center of the laser pulse, to within  $\pm 50$  ps. The instrument was located to detect SRS sidescatter, being  $135^\circ$  from the wave vector and  $90^\circ$  from the electric field vector of the incident laser light.

Figure 3 shows lineouts of data from this instrument for a shot with an intensity of  $4 \times 10^{15}$  W/cm<sup>2</sup>, which

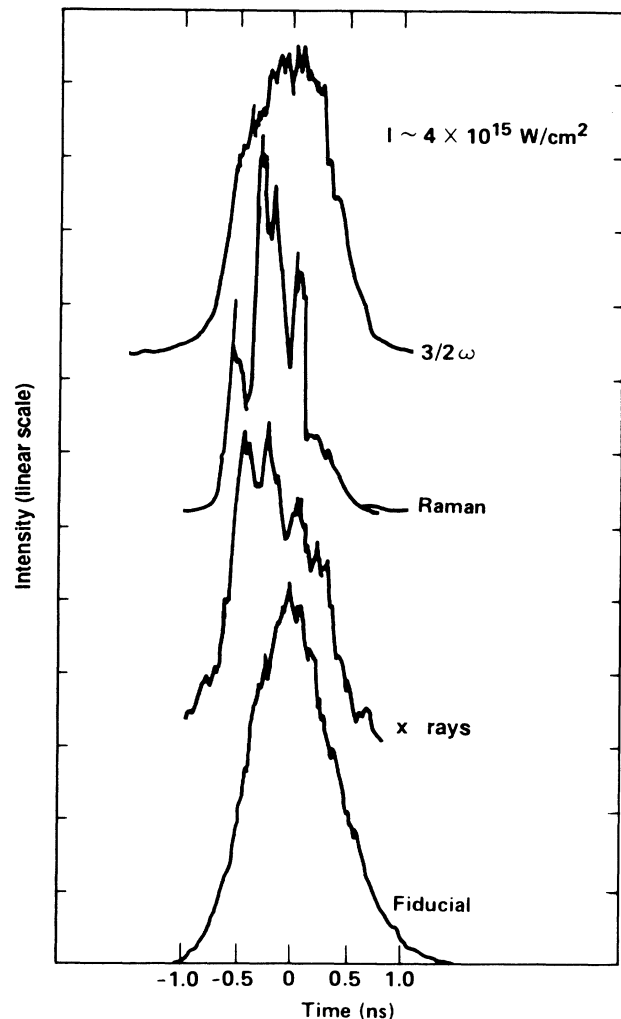


FIG. 3. Results from the optical x-ray streak camera. A laser fiducial, the SRS light, the light at  $\frac{3}{2}\omega_0$ , and the hard x-ray emission are shown (in arbitrary units on a linear scale), as a function of time from experiment 94020303.

produced a significant hard x-ray signal. The figure shows relative intensity in each channel versus time, on linear scales. The onset of the SRS, the  $\frac{3}{2}\omega_0$ , and the x rays is nearly simultaneous on this relatively high intensity shot. The bursts in the SRS at this angle may correspond to the fluctuations in the x-ray spectra in the figure. Because the SRS occurs at many angles, we would expect at best a partial correlation. (The fluctuations in the  $\frac{3}{2}\omega_0$  signal are about the size of the noise in the instrument.) The x rays drop to half their peak intensity after the SRS at this angle, but before the  $\frac{3}{2}\omega_0$ . Thus, the x ray timing is consistent with SRS as the source of the x rays but does not rule out other mechanisms.

#### IV. THE HOT-ELECTRON TEMPERATURE AND FRACTION

For each of the target irradiations reported here, the temperature and energy content of the hot electrons were determined. The temperature,  $T_h$ , of the hot electrons was taken to be that of the x-ray spectrum. The energy content of the hot electrons in J,  $E_h$ , was determined from the spectral intensity  $\Omega$  at an x-ray energy  $E_x = T_h$ , using

$$\Omega[\text{keV}/(\text{keV } 4\pi \text{ sr})] = 5 \times 10^{11} E_h (Z/79),$$

where  $Z$  is the nuclear charge of the target material. This analysis of the x-ray spectrum has been used in several other papers<sup>10,13,15,17</sup> but its justification has never been described in print. We have included an Appendix to rectify this omission.

Figure 4 shows the hot-electron temperature  $T_h$  as a

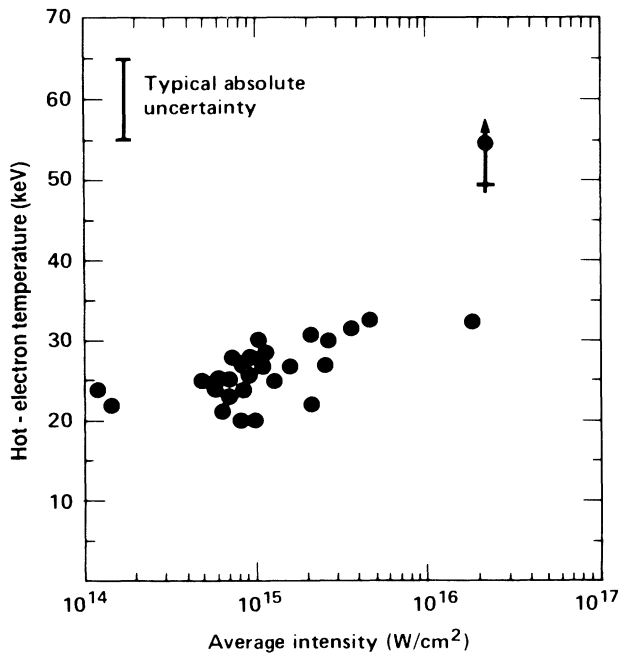


FIG. 4. The temperature of the hot electrons, inferred from the x-ray data as described in the text, is plotted as a function of the average laser intensity incident on the target. The typical absolute uncertainty is indicated.

function of the average laser intensity  $I_L$  incident on target. The scatter in the data is about  $\pm 20\%$ , which corresponds to the uncertainty in the measurement. The temperature appears to increase slowly with intensity. Any power-law dependence is difficult to discern from the data, which show that  $T_h$  increases less rapidly than  $I_L^{0.2}$ . Based on plasma simulations,<sup>18</sup> a rough estimate of the temperature of the hot electrons produced by electron-plasma waves is  $kT_h = \frac{1}{2}m_e v_{ph}^2$ , where  $v_{ph}$  is the phase velocity of the electron-plasma waves,  $k$  is the Boltzmann constant, and  $m_e$  is the electron mass. Based on the observed SRS spectra and angular distributions, the range of phase velocities of the electron-plasma waves produced by SRS corresponded to hot-electron temperatures of 14 to 40 keV. Thus SRS could easily have produced an average  $T_h$  of 20 to 30 keV. In addition, the small variation of  $T_h$  with intensity is consistent with SRS. In contrast, resonance absorption and two-plasmon decay are unlikely to have produced the observed  $T_h$ . Resonance absorption would be expected to produce a more rapid increase of  $T_h$  with  $I_L$ ; the mean hot-electron energy produced by resonance absorption is predicted<sup>2,19,20</sup> and observed<sup>21,22</sup> to scale as  $I_L^{0.3}$  to  $I_L^{0.5}$ .

Two-plasmon decay would be expected to produce values of  $T_h$  more than twice those observed (about 70 versus 25 keV). However, the scaling with laser intensity of the  $T_h$  produced by two-plasmon decay is expected and has been observed<sup>22,23</sup> to be weak. The discrepancy with regard to the value of the temperature indicates that two-plasmon decay is not responsible for the hot electrons but is not conclusive. The relation of the hot-electron temperature to the plasma wave properties is not understood in sufficient detail to be certain of discrepancies as small as a factor of 2 or 3. Past experiments in which hot-electron production has been attributed to two-plasmon decay have found the temperature to be comparable to<sup>22,23</sup> higher than,<sup>24</sup> or lower than<sup>22,25</sup> that expected from the plasma-wave phase velocity.

Figure 5 shows the hot-electron fraction  $f_h$  as a function of  $I_L$ , where  $f_h$  is the ratio of  $E_h$  to the energy of the laser light incident on the target. The  $f_h$  increased much more than the uncertainty in its determination as  $I_L$  increased from  $1 \times 10^{14}$  to  $4 \times 10^{15}$  W/cm<sup>2</sup>. It reached a few percent at the highest laser intensities. The scatter in  $f_h$ , at intensities near  $10^{15}$  W/cm<sup>2</sup>, is larger than the uncertainties in  $f_h$  and  $I_L$ . This suggests that the hot-electron production depends on the detailed properties of the laser beam and the plasma, which may vary from one experiment to the next.

In contrast, the quantitative and qualitative variations of the SRS correspond very well to those of the hot electrons. Figure 6 shows  $f_h$  as a function of the fraction of the laser light scattered as SRS light  $f_R$ . We see that, within the uncertainties, these two quantities are very well correlated as they vary by more than 2 orders of magnitude. The line in the figure shows the fraction of the laser energy converted into electron-plasma waves as a function of  $f_R$ , based on the observed spectrum of the SRS light. Within the uncertainties, the line intersects all the data. This suggests that the dominant energy-loss

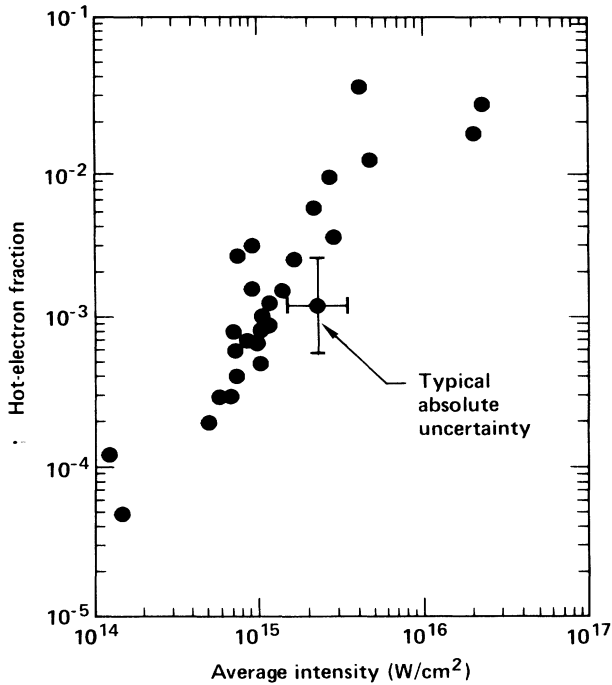


FIG. 5. The fraction of the laser energy converted into hot electrons, inferred from the x-ray data as described in the text, is plotted as a function of the average laser intensity incident on the target. The typical absolute uncertainty is indicated.

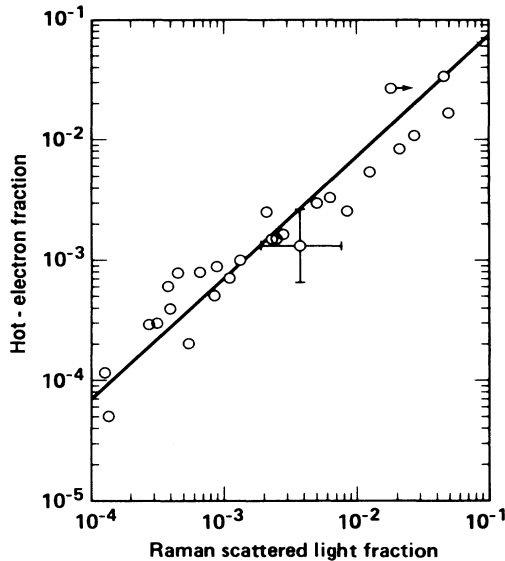


FIG. 6. The fraction of the laser energy converted into hot electrons is plotted as a function of the fraction of the laser energy scattered as SRS light. The typical absolute uncertainty is indicated. The line shows the energy inferred from the SRS fraction and spectrum to have been present in the electron-plasma waves, which produce hot electrons by Landau damping.

mechanism for the electron-plasma waves is Landau damping, and is further evidence that the SRS is responsible for the hot electrons. Note that there is some tendency for  $f_h$  to lie above the curve when  $f_R$  is low. This may reflect hot-electron production by two-plasmon decay, which has previously been observed at comparable levels.<sup>22</sup> A linear-regression, power-law fit of  $f_h$  to  $f_R$  gives a power of  $0.88 \pm 0.06$  and the rms deviation of the data from this curve is a factor of 1.6, which is less than the uncertainty of the data.

A number of experiments<sup>22,23,25,26</sup> have measured the efficiency of hot-electron production under conditions in which two-plasmon decay was well above threshold while Raman scattering was quite weak. In every such case, at laser wavelengths from 0.35 to 1.06  $\mu\text{m}$ ,  $f_h$  has been directly proportional to the fraction of the laser energy scattered as  $(\frac{3}{2})\omega_0$  light,  $f_{3/2}$ . Thus, in spite of the fact that the  $(\frac{3}{2})\omega_0$  light is produced by only a fraction of the plasma waves driven by two-plasmon decay, it appears to be a good indicator of the integrated energy converted into electron-plasma waves by two-plasmon decay. In the present experiment, for which we attribute the production of hot electrons to Raman scattering,  $f_h$  is not directly proportional to  $f_{3/2}$ , as Fig. 7 shows. A linear-regression fit of  $f_h$  to  $f_{3/2}$  gives a power of  $1.58 \pm 0.18$  and the rms deviation of the data from this curve is 2.2, which is larger than the uncertainty of the data.

Consideration of Fig. 6, Fig. 7, and previous data gives one several reasons to conclude the hot electrons are dominantly the result of SRS rather than two-plasmon decay, particularly when  $f_h$  is large. First, the previous paragraph that discussed Fig. 6 showed that the hot-electron data are *quantitatively* as expected from the Raman data, with perhaps a small contribution from two-plasmon decay at low  $f_h$ . Second, the scaling of  $f_h$  with  $f_{3/2}$  shown in Fig. 7 is different from that observed in previous experiments in which hot-electron production has been attributed to two-plasmon decay. Third, the rms deviation of the data in Fig. 7 from the power-law fit

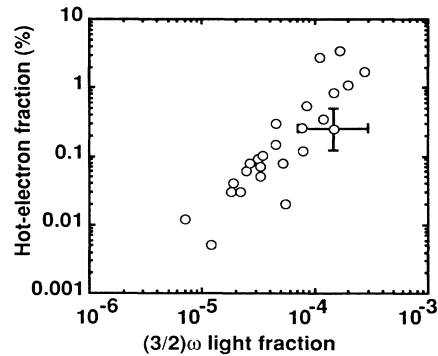


FIG. 7. The fraction of the laser energy converted into hot electrons is plotted as a function of the fraction of the laser energy scattered as  $(\frac{3}{2})\omega_0$  light. The typical absolute uncertainty is indicated.

is larger than the uncertainty in the data, in contrast to the result for Fig. 6.

## V. DISCUSSION

All the evidence is consistent with the hypothesis that SRS produces the hot electrons. First, the magnitude and slope of the x-ray spectrum is quantitatively as expected from the observed SRS, assuming the plasma waves convert all their energy to hot electrons. Second, the timing of the x rays is consistent with that of the SRS. Third, the variation of the x-ray amplitude (and inferred hot-electron fraction) tracks that of the SRS amplitude over more than 2 orders of magnitude, both as the laser intensity changes in the Novette experiments and as the scalelength changes by comparison with experiments from Argus.

One or more pieces of evidence weighs against every other mechanism that might produce hot electrons. Two-plasmon decay should produce (and has produced) a larger hot-electron temperature than is observed; the hot electron fraction is less well correlated with the  $(\frac{3}{2})\omega_0$  emission than with the SRS as laser intensity and density scalelength vary; and the slope of the best-fit scaling of the hot-electron fraction with the  $(\frac{3}{2})\omega_0$  emission is larger than would be expected if the two-plasmon decay instability were responsible for the hot electrons. Second, mechanisms near critical density (resonance absorption, parametric decay, or cavitation resulting from these) should be less evident in the long scalelength plasmas produced in the Novette experiments than they were in those of Argus or other similar experiments. In addition, the temperature of the hot electrons produced by these mechanisms is lower than that observed here and scales differently with laser intensity. Third, the relatively long scalelength of the plasmas discussed here might, in principle, be overcome by very strong filamentation. This could enhance the SRS, but might also enhance two-plasmon decay or critical-surface phenomena. If the filamentation were so strong as to be saturated in all these experiments, then the x-ray and scattered-light emissions ought to be relatively independent of average laser intensity, because the strongest laser-plasma interactions would occur within the filaments. In contrast, the data show a very strong intensity dependence.

In conclusion, the measurements of hard x-ray and scattered-light emissions reported here provide a compelling case that stimulated Raman scattering is responsible for the hot-electron generation in, and consequent hard x-ray emission from, the plasmas under consideration. The plasmas are relatively planar, with scale lengths of several hundred laser wavelengths, and with densities and temperatures that are relevant to laser fusion. The laser intensities are also relevant to laser fusion. If hot electron fractions above 1% (as observed here) were produced in a high gain target, and if their energy were efficiently coupled into the fuel, then the gain of the target would be significantly reduced. Further studies of hot-electron production and transport in laser-produced plasmas will be necessary to accurately assess the threat they may pose to laser fusion.

## ACKNOWLEDGMENTS

The authors acknowledge the support of Ed McCauley in analyzing the hard-x-ray spectra and useful discussions with Dr. R. L. Kauffman and Dr. D. W. Phillion. In addition, these experiments would not have been possible without the sustained efforts of the scientific, technical, and clerical personnel in the areas of Novette Laser Operations, Target Fabrication, and Target Diagnostics. Work performed under the auspices of the U.S. Department of Energy by the Lawrence Livermore National Laboratory under Contract No. W-7405-ENG-48.

## APPENDIX: ANALYSIS OF X-RAY SPECTRA

This appendix describes our calculation of the relation between the energy content and the temperature of the hot electrons and the measured x-ray spectra, and some of the caveats that apply. The calculation assumes that the electron distribution function is Maxwellian over a sufficient range of energies and is based upon the properties of thick-target bremsstrahlung emission by a Maxwellian distribution of electrons. Both measurements of the electrons emitted by laser-irradiated plasmas<sup>11,27</sup> and simulations<sup>18</sup> have generally observed Maxwellian distributions of electrons, so this assumption is not unreasonable. However, the analysis cannot guarantee that the electron distribution is actually Maxwellian.

The calculation of the x-ray spectrum proceeds as follows. The energy radiated per unit frequency interval and into  $4\pi$  steradians by an energetic electron as it slows down in a thick target is known and has been measured.<sup>28</sup> When this expression is integrated over a Maxwellian distribution of electrons, one finds that the resulting x-ray spectrum decays with x-ray energy  $E_x$  as  $\exp(-E_x/T_h)$ , where  $T_h$  is the temperature of the Maxwellian distribution of electrons. Thus, the "temperature" inferred from the x-ray spectrum in Sec. II can be taken to be the temperature of the hot electrons,  $T_h$ . One also finds that the spectral intensity  $\Omega$  at an x-ray energy  $E_x = T_h$ , is as given in Eq. (1) of the text. The electron distribution function in a real target is generally taken to be piecewise Maxwellian, producing a piecewise exponential x-ray spectrum that can be analyzed as the sum of two or more spectra of the form and magnitude just described.

This calculation was tested in two ways, both of which gave the same result as Eq. (1) to within a factor of 2. First, the Bethe-Heitler cross section was used to calculate the emission of x rays by an electron (by electron-ion collisions) while the electron loses energy via electron-electron collisions. This result was then integrated over a Maxwellian distribution. Second, the x-ray spectrum produced by a Maxwellian distribution of hot electrons was calculated using the LASNEX (Ref. 29) computer code, which includes improved cross sections for the bremsstrahlung emission and properly distinguishes between bound and free electrons when computing the energy loss. In addition, similar calculations, with similar results, have been reported by others.<sup>30</sup> Finally, even if

the inference of the energy content of the hot electrons from the x-ray spectrum were perfect, it would only reveal the energy that is lost in the thick target. This measurement cannot detect any energy the hot electrons lose before reaching the thick target, such as to hydrodynam-

ic expansion. Based on all the above considerations, we assign an absolute uncertainty of a factor of 2 to the energy content of the hot electrons inferred from the measured x-ray spectrum. The relative uncertainty is smaller but is equally difficult to quantify.

- 
- <sup>1</sup>R. P. Drake, R. E. Turner, B. F. Lasinski, E. A. Williams, D. W. Phillion, K. G. Estabrook, W. L. Kruer, E. M. Campbell, K. R. Manes, J. S. Hildum, and T. W. Johnston, *Phys. Fluids* **31**, 3130 (1988).
- <sup>2</sup>J. P. Freidberg, R. W. Mitchell, R. L. Morse, and L. I. Rudinski, *Phys. Rev. Lett.* **28**, 795 (1972).
- <sup>3</sup>T. Speziale and P. J. Catto, *Phys. Fluids* **20**, 990 (1977).
- <sup>4</sup>F. W. Perkins and J. Flick, *Phys. Fluids* **14**, 2012 (1971).
- <sup>5</sup>E. A. Jackson, *Phys. Rev.* **153**, 235 (1967).
- <sup>6</sup>A. B. Langdon, B. F. Lasinski, and W. L. Kruer, *Phys. Rev. Lett.* **43**, 133 (1979).
- <sup>7</sup>V. E. Zakharov, in *Handbook of Plasma Physics*, edited by M. N. Rosenbluth and R. Z. Sagdeev (Elsevier, New York, 1984), Vol. 2, p. 81; *Basic Plasma Physics II*, edited by A. A. Galeev and R. N. Sudan (Elsevier, New York, 1984).
- <sup>8</sup>C. S. Liu, M. N. Rosenbluth, and R. B. White, *Phys. Fluids* **17**, 1211 (1974).
- <sup>9</sup>R. P. Drake, *Commun. Plasma Phys. Controlled Fusion* **XII**, 181 (1989).
- <sup>10</sup>D. W. Dillon, D. L. Banner, E. M. Campbell, R. E. Turner, and K. G. Estabrook, *Phys. Fluids* **25**, 1434 (1982).
- <sup>11</sup>C. Joshi, T. Tajima, J. M. Dawson, H. A. Baldis, and N. A. Ebrahim, *Phys. Rev. Lett.* **47**, 1285 (1981).
- <sup>12</sup>R. Berger, R. D. Brooks, and Z. A. Pietrzyk, *Phys. Fluids* **26**, 354 (1983).
- <sup>13</sup>R. P. Drake, R. E. Turner, B. F. Lasinski, K. G. Estabrook, E. M. Campbell, C. L. Wang, D. W. Phillion, E. A. Williams, and W. L. Kruer, *Phys. Rev. Lett.* **53**, 1739 (1984).
- <sup>14</sup>K. R. Manes, O. C. Barr, E. S. Bliss, R. P. Drake, R. O. Godwin, D. G. Gritton, J. S. Hildum, F. W. Holloway, C. A. Hurley, B. C. Johnson, D. J. Kuizenga, B. Merritt, R. G. Ozarski, R. Reinecker, Jr., J. R. Severyn, D. R. Speck, M. A. Summers, G. J. Suski, and E. P. Wallerstein, *Laser Part. Beams* **3**, 173 (1985).
- <sup>15</sup>W. C. Mead, E. M. Campbell, K. G. Estabrook, R. E. Turner, W. L. Kruer, P. H. Y. Lee, B. Pruett, V. C. Rupert, K. G. Tirsell, G. L. Stradling, F. Ze, C. E. Max, M. C. Rosen, and B. F. Lasinski, *Phys. Fluids* **26**, 2316 (1983).
- <sup>16</sup>R. E. Turner, D. W. Phillion, E. M. Campbell, and K. G. Estabrook, *Phys. Fluids*, **26**, 579 (1983).
- <sup>17</sup>M. D. Rosen, D. W. Phillion, V. C. Rupert, W. C. Mead, W. L. Kruer, J. J. Thomson, N. H. Kornblum, V. W. Slivinsky, G. J. Caporaso, and M. J. Boyle, and K. G. Tirsell, *Phys. Fluids* **22**, 2020 (1979).
- <sup>18</sup>Kent Estabrook, W. K. Kruer, and B. F. Lasinski, *Phys. Rev. Lett.* **45**, 1399 (1980).
- <sup>19</sup>D. W. Forslund, J. M. Kindel, and K. Lee, *Phys. Rev. Lett.* **39**, 284 (1977).
- <sup>20</sup>Kent Estabrook and W. L. Kruer, *Phys. Rev. Lett.* **40**, 42 (1978).
- <sup>21</sup>D. C. Slater, Gar. E. Busch, G. Charatis, R. R. Johnson, F. J. Mayer, R. J. Schroeder, J. D. Simpson, D. Sullivan, J. A. Tarvin, and C. E. Thomas, *Phys. Rev. Lett.* **46**, 1199 (1981).
- <sup>22</sup>R. L. Keck, L. M. Goldman, M. C. Richardson, W. Seka, and K. Tanaka, *Phys. Fluids* **27**, 2762 (1984).
- <sup>23</sup>D. M. Willeneuve, R. L. Keck, B. B. Afeyan, W. Seka, and E. A. Williams, *Phys. Fluids* **27**, 721 (1984).
- <sup>24</sup>J. Meyer and H. Houtman, *Phys. Fluids* **28**, 1549 (1985).
- <sup>25</sup>F. C. Young, M. J. Herbst, C. K. Manka, S. P. Oenschain, and J. H. Gardner, *Phys. Rev. Lett.* **54**, 2509 (1985).
- <sup>26</sup>L. M. Goldman, W. Seka, K. Tanaka, R. W. Short, and A. Simon, *Can. J. Phys.* **64**, 969 (1986).
- <sup>27</sup>H. Figueroa, C. Joshi, H. Azechi, N. A. Ebrahim, and K. G. Estabrook, *Phys. Fluids* **27**, 1887 (1984).
- <sup>28</sup>A. H. Compton and S. K. Allison, *X-rays in Theory and Experiment* (Van Nostrand, London, 1935), p. 105.
- <sup>29</sup>G. B. Aimmerman and W. L. Kruer, *Commun. Plasma Phys. Controlled Fusion* **2**, 85 (1975).
- <sup>30</sup>K. A. Brueckner, *Phys. Rev. Lett.* **36**, 677 (1976); **37**, 1247 (1976); D. B. Henderson and M. A. Stroschio, *ibid.* **37**, 1244 (1976).